IEEE Access
Multidisciplinary | Rapid Review | Open Access Journal

Received December 6, 2019, accepted December 17, 2019, date of publication December 23, 2019,
date of current version December 31, 2019.

Digital Object Identifier 10.1109/ACCESS.2019.2961509

A Simplified Extension of Physics-Based Single Particle Model for Dynamic Discharge Current

JINGLONG CHEN, RIXIN WANG, YUQING LI, And MINQIANG XU
Deep Space Exploration Research Center, Harbin Institute of Technology, Harbin 150001, China

Corresponding author: Rixin Wang (wangrxhit@163.com)

This work was supported by the Key Laboratory Opening Funding from Harbin Institute of Technology under Grant HIT.KLOF.2018.076.

ABSTRACT The prediction of the battery temperature and terminal voltage under dynamic load condition is crucial for a satellite battery management system. Restricted by parameter measurability and computing resources, equivalent circuit model has been commonly used in battery management system. But this model cannot satisfy the necessary performance under dynamic load for usual work of satellites. On account of this problem, a combined temperature single particle model is developed for 18650 cells in this paper. The proposed model consists of two sub-models, an electrochemical model and a thermal model, which are coupled together in an iterative manner through physicochemical temperature dependent parameters. The electrochemical sub-model mainly simplifies the calculation of lithium-ion concentration in electrode, while an expression for battery temperature distribution is employed in the thermal sub-model. In addition, genetic algorithm is adopted to estimate model parameters by exciting the battery under different operation conditions. This proposed model can provide accurate predictions of terminal voltage and surface temperature at various operating conditions and the proper simplification of mathematical structure making it ideal for real-time battery management system application. Finally, the model is validated against both constant and dynamic load conditions.

INDEX TERMS Battery management systems, mathematical model, satellites, thermal analysis.

I. INTRODUCTION

Battery is a critical component for energy storage in spacecraft. It stores the excess power produced by solar cells in the sun, and provides the electricity to spacecraft in the dark. For the battery of satellite, typical cycle-life target is 5 years (30,000 cycles) for Low Earth Orbit (LEO) and 15 years (1350 cycles) for Geosynchronous Earth Orbit (GEO) [1]. Thus, due to the requirements of long-life and high energy density, Lithium-ion battery have been widely adopted by new generation of satellites.

The operation safety of lithium-ion battery and prolongation of battery serve life are relied heavily on battery management system (BMS) [2]. With respect to the lithium-ion battery of satellite, two distinct characteristics (high capacity and large serial parallel numbers) would cause several problems such as safety, durability and uniformity. The changing discharge current, depth of discharge, and ambient temperature (*AT*) would cause large monitoring errors of battery state including capacity and resistance. Besides, BMS should prevent over-charge and over-discharge which could induce rapid attenuation of battery performance, and adjust work strategy to prolong battery life [3]. Therefore, satellite BMS needs accurate and efficient models to control current and temperature for single battery under the request of low discharge current and variable work condition.

In existing literatures, electrical model and electrochemical model have appeared as two main models in the fields of state monitoring and prediction of battery. The electrical model such as equivalent circuit model (ECM) is widely used in satellite BMS due to its simplicity and low computational cost [4]. Thevenin model is one of the most common models for state of charge (*SOC*) estimation and battery simulation. It is usually composed of one open circuit voltage source and one or two resistor-capacitor (RC) networks [5]. Classic Thevenin model uses one voltage source to represent battery open-circuit voltage (*OCV*), one resistance to represent ohmic polarization which is equal direct current resistance (*DCR*), and two RC networks to describe the phenomenon of concentration polarization and activation polarization respectively. One RC networks representing activation polarization could be simplified as resistance and merged into ohmic resistance

The associate editor coordinating the review of this manuscript and approving it for publication was Ziang Zhang.

because activation polarization will be equilibrium in milliseconds. The other RC network representing concentration polarization gives Thevenin model the ability to approximately reflect the response of dynamic loading. This means that the dynamic process of voltage only depends on current. It will bring large error to the battery model especially under dynamic loading. For example, the voltage could rise after discharge stops, and this process not only depends on current but also relates to *SOC* and temperature. This phenomenon obviously reflects the limitation of Thevenin model. This disadvantage can be mitigated by constructing the relation between resistor, capacitor and *SOC*, state of health (*SOH*) and temperature [6], [7], yet the model built by this manner is still labor-intensive and time-consuming and usually has low generalization ability to new batteries [8]. So, the electrical model cannot completely satisfy the satellite BMS.

Electrochemical model accurately describes the discharge behavior of lithium-ion battery through analyzing physical phenomena such as the transport and diffusion of charges and lithium-ions [9]. The pseudo-two-dimensional (P2D) model describes the lithium salt transport phenomenon in the electrolyte and solid phases, and captures charge transfer reaction in the positive and negative porous electrodes [10]. With the full mechanism's description and highly precise, P2D model has already become one of the most common models in electrochemical model, and it has been widely used in researching electrochemical parameters of battery including the electrolyte concentration, electrolyte potential, solid-state potential, and solid-state concentration [11]. Rigorous P2D model uses coupled nonlinear partial differential equations to exactly describe internal chemical processes of batteries, and that would take seconds to minutes to simulate every time step. In order to improve computational efficiency, many researches have simplified and improved the P2D model, such as Dao *et al*. [12] used several techniques such as volume-averaging, Galerkin's method and curve-fitting to simplify P2D model. Yuan *et al*. [13] simplified the computation process through modifying boundary condition and adopting Padé approximation method. Ma *et al*. [14] also adopted dimensionality reduction and Padé approximation to build a simplified one-dimensional Lithium-ion battery model.

Single particle model (SP) also evolves from P2D model. It assumes that in an electrode the local volumetric transfer current density is constant and equals to the average value. That means that all the pore wall fluxes of particles are the same. Besides, this model assumes that all the particles in an electrode follow the same behavior and the current passed through the electrode is uniformly distributed over all the particles. Consequently, each electrode is modeled as two spherical particles in which intercalation and de-intercalation phenomena occur, and the effects of concentration and potential in the solution phase between the particles have been neglected [15]. Due to these assumptions, SP model is very simple and requires low computational cost. And the accuracy of the SP model is acceptable under low current [16]. Therefore, it has been applied to online estimation [17] and life analysis [18]–[20].

Temperature has a significant impact on battery behavior. The main reason is that some electrochemical parameters are sensitive to temperature, such as diffusion coefficient and resistance. Northrop *et al*. [21] researched temperature profile of main parameters and proposed a simple P2D model. Damay *et al*. [22] analyzed the thermal behavior of battery and proposed a heat sources model. Wang *et al*. [23] simplified the heat sources model and combined with finite-element method to effectively track surface temperature of battery. Then, Farag *et al*. [24] further analyzed heat effect and developed a combined electrochemical, heat generation and thermal model.

Although there have been abundant research works in model simplification, the great computational cost is still the primary obstacle for its application on satellite BMS which hold limited computation resource. Meanwhile, electrochemical model needs more than 16 electrochemical parameters [12], some of which are unmeasured or unmeasurable and will prevent the application of electrochemical model in satellite BMS.

In general, electrochemical model has the highest accuracy but the largest complexity, while ECM is simple but has low accuracy. To balance complexity and accuracy, a united model of electrochemical model and electrical model has been studied recently. Prasad and Rahn [25] deduced the parameters of electrical model (resistance and capacitance) from single partial model. Liu *et al*. [26] employed Butler-Volmer equation-based electrical model to capture the voltage change induced by changing rates for the high-power lithium battery. Zhang *et al*. [27] deduced the parameters of electrical model (Open cycle voltage, resistance, and capacitance) from P2D model. These methods have improved the estimation accuracy of model parameters, but cannot handle the issue under dynamic current response.

The satellite battery discharge current and ambient temperature are always changing periodically. In general, the battery discharge current is below 0.5C, and the ambient temperature keeps within specified bounds. So, to predict battery behavior more accurate and efficient under both static and dynamic loading conditions, a combined temperature single particle model (CTSPM) for discharge has been proposed in this paper. This model can predict the voltage of battery considering the effects of temperature and loadings. Further, the proposed model can predict the end of discharge. Compared with electrical model, it has higher precision by considering the dynamic concentration and the impact of temperature. Compared with electrochemical model, this model simplifies the SP model through average volume [28] and obtains the electrode potential through look-up table. Then, concentration is calculated by Fick's law of diffusion. Thus, this model neglects the information of lithium-ion concentration distribution and potential distribution which are unnecessary for satellite BMS, and its computational speed is very fast. Particularly, combining with the degradation of parameters,

CTSPM can capture battery state of health and predict the remaining useful life of battery.

This paper is organized as follows. In Section II, the structure of CTSPM is described, In Section III, a simplified electrochemical model is established. In Section IV, heat generation has been analyzed and simplified thermal model is established. In section V, the experimental process has been described and genetic algorithm is employed to identify parameters of model. In Section VI, the simulation and experiment results are given along with detailed analysis. The conclusions are drawn finally in Section VII.

II. CTSPM STRUCTURE

This section will present the main contributions of this paper, i.e., how the CTSPM allows BMS to operate the battery effectively in safe conditions and improve its prediction accuracy of terminal voltage and surface temperature under dynamic current condition. Fig. 1 shows a schematic representation of CTSPM and its sub-models. The CTSPM is capable of simulating cell terminal voltage and surface temperature. It is divided into two different sub-models including electrochemical model and thermal model.

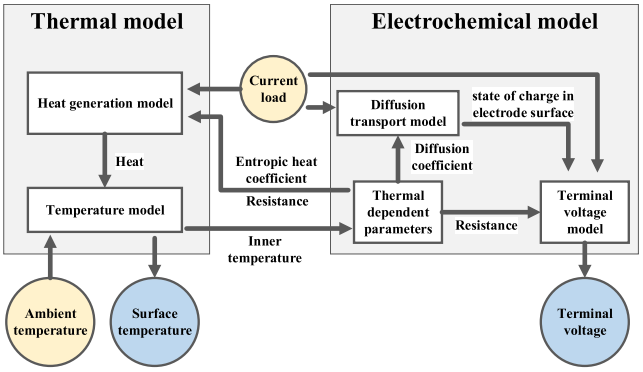

FIGURE 1. Schematic diagram for CTSPM.

Firstly, the electrochemical model describes cells terminal voltage under low current (usually less than the 1C rate, where the "1C" rate refers to a rate at which the battery will be discharged to empty in an hour after fully charged at room temperature) as a function of the electrode surface state of charge. To quickly obtain the electrode surface state of charge, a simplified lithium-ion diffusion transport model has been proposed. In the electrochemical model, both lithium-ion diffusion coefficient and resistance are sensitive to temperature, and the effect of temperature is described by Arrhenius equation.

Secondly, the thermal model calculates the inner temperature, and the obtained inner temperature is fed back to the electrochemical model as an input. Reversible and irreversible heat have been considered as a function of the measured current, the *SOC*, and the resistance. Then, the temperature model evaluates the inner temperatures as a function of heat generation rate, ambient temperature, cell geometry, and boundary conditions. Meanwhile, an empirical formula has been employed to output surface temperature.

In Fig. 1, the yellow circles represent inputs and the blue circles represent outputs. The colored-doted blocks represent software functions. The CTSPM inputs are data provided by the sensors, and the outputs are processed data transferred to the main BMS.

In this section, the general formulation of the CTSPM is presented. In the following sections, the two sub-models are discussed in details.

III. ELECTROCHEMICAL MODEL

A. TERMINAL VOLTAGE MODEL

In fact, concentration polarization reflects the change of potential caused by variation of electrolyte concentration. Assuming that the temperature is constant in the SP model, then, the electrode potential is the function of the concentration of Li^+ ions in the intercalation particle of electrode. So, the terminal voltage V_t is different between two electrode potentials and can be rewritten as [29]

$$V_t = U_p\left(\theta_p\right) - U_n\left(\theta_n\right) - R_\Omega I \tag{1}$$

where I is the battery load current, U_k, $k = n, p$ is the electrode potential. The subscripts n and p to denote the negative electrode and the positive electrode, respectively. θ_k, $k = n, p$ is the electrode surface state of charge and it is a function of the normalized surface concentration

$$\theta_k = c_{s,k,surf}/c_{s,k,surf}^{\max} \tag{2}$$

where $c_{s,k,surf}$, $k = n, p$ is the concentration of Li^+ ions in the electrode surface, $c_{s,k,surf}^{\max}$, $k = n, p$ is the maximum concentration of Li^+ ions in the electrode surface. R_Ω is the total resistance

$$R_\Omega = \frac{1}{A}\left(\frac{\delta_p}{2\kappa_p} + \frac{\delta_{sep}}{2\kappa_{sep}} + \frac{\delta_n}{2\kappa_n} - \frac{RT_{in}}{a_p\delta_p i_{0,p}F} + \frac{RT_{in}}{a_n\delta_n i_{0,n}F}\right) + R_f + R_c \tag{3}$$

where A is the area of electrode, R is universal gas constant, F is Faraday constant, T_{in} is the inner temperature of battery, a_p is the specific contact area of the positive, a_n is the specific contact area of the negative, δ_p, δ_n and δ_{sep} denote the thicknesses of positive, negative and separator element, respectively. κ_p, κ_n and κ_{sep} represent the effective conductivity in the positive, negative, and separator element, respectively. R_f is the film resistance at interphase, and R_c is the resistance at the current collectors. $i_{0,k}$, $k = n, p$ is the exchange current density at cell edges [30]

$$i_{0,k} = Fk_{eff}\left[c_{e,k}\left(x,t\right)\right]^{\alpha_a}\left[c_{s,k,surf}\left(x,t\right)\right]^{\alpha_c} \cdot \left[c_{s,k,surf}^{\max} - c_{s,k,surf}\left(x,t\right)\right]^{\alpha_a} \tag{4}$$

where $c_{e,k}$ is the electrolyte concentration, k_{eff} is the reaction rate constant, α_a and α_c are the transfer coefficient. In the SP model, the constant electrolyte concentration assumption has been validated for lower rates (<1C), and both transfer

coefficient α_a and α_c can be set as 0.5 in general [31]. Then, (4) can be rewritten as

$$i_{0,k} = \kappa_k \sqrt{\theta_k \left(1 - \theta_k\right)} \tag{5}$$

where $\kappa_{=} F c_{e,k} c_{s,k,surf}^{\max} k_{eff}$. Substituting (3) and (5) into (1), the terminal voltage is rewritten as

$$V_t = U_p\left(\theta_p\right) - U_n\left(\theta_n\right) - R_\Omega\left(\theta_p, \theta_n\right) I \tag{6}$$

Because lithium-ion transfer obeys the second Fike's law, and the two electrodes have a symmetric initial condition and boundary condition, the state of charge in electrode surface θ_k can be described as

$$\theta_p = I \cdot t / q_{s,p,\max} \tag{7}$$

$$\theta_n = 1 - I \cdot t / q_{s,n,\max} \tag{8}$$

where $q_{s,k,max}, k = n, p$ is the maximum active charge in the electrode surface which can be calculated by

$$q_{s,k,\max} = q_{\max} \frac{v_{s,k}}{v_k} \tag{9}$$

where $q_{\max}, k = n, p$ is the maximum active charge in the electrode, $v_{s,k}, k = n, p$ is the volume of the electrode surface part which is interpreted in Section III.B, $v_k, k = n, p$ is the volume of the electrode. In this paper, we assumed that $q_{p,\max} = q_{n,\max}$, $v_{s,p} = v_{s,n}$, and $v_p = q_n$. $q_{\max}$ is the maximum active charge in battery which can be expressed by the function of battery capacity $C_{battery}$

$$q_{\max} = 3600 \cdot C_{battery} \tag{10}$$

According to (7)-(9), θ_n can be represented as

$$\theta_n = 1 - \theta_p \tag{11}$$

Thus, finally, terminal voltage is described as the function of the positive electrode surface state of charge

$$V_t = G\left(\theta_p\right) - R_\Omega\left(\theta_p\right) I \tag{12}$$

At a small current condition (<1/20C), the lithium-ion concentration gradient can be neglected and the lithium-ion concentration in the electrode follows a uniform distribution. Under these simplifications, the surface concentration is equal to the average concentration approximately. That means θ_p is equal to battery *SOC* under equilibrium state. So, the curve $V_{oc} = G(\theta_p)$ can be measured by the small current discharge test (1/20C) and would be used through the look-up table method.

Resistance is also a function of θ_p. Yang's *et al.* [32] indicated that the resistance rapidly increases with the depth of discharge. This law works in all stages of battery degradation. The aging experiment also indicates that *DCR-SOC* curves in different degradation stages keep the same shape and overall increase with aging. Therefore, for estimating the resistance under different *SOH*, the function R_Ω can be represented as

$$R_\Omega = R_0 + H\left(\theta_p\right) \tag{13}$$

where R_0 is the resistance at $SOC = 1$, $H(\theta_p)$ is a shape function that can be obtained through the look-up table method.

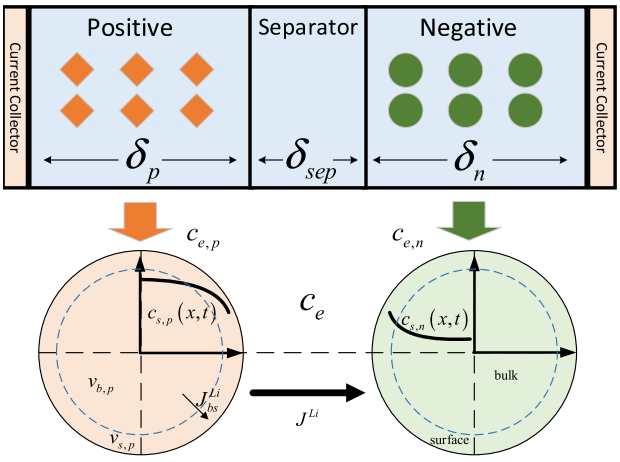

FIGURE 2. Concept of SP model simplification.

In this paper, $H(\theta_p)$ is one of *DCR-SOC* curve divide by resistance at $SOC = 1$

B. SIMPLIFIED LITHIUM DIFFUSION TRANSPORT MODEL

As Fig. 2 shows, the SP model neglects the effects of concentration and potential in the electrolyte phase, and assumes that each electrode is modeled as one spherical particle. That means lithium-ions move from the positive electrode to the negative electrode indirectly and the lithium-ion concentration in the solid phase for each electrode is described by the radial diffusion equation

$$\frac{\partial c_k}{\partial t} = D \frac{1}{r^2} \frac{\partial}{\partial r}\left(r^2 \frac{\partial c_k}{\partial r}\right) \tag{14}$$

with boundary condition

$$\left.\frac{\partial c_k}{\partial r}\right|_{r=0} = 0\,, \quad \left.\frac{\partial c_k}{\partial r}\right|_{r=R_k} = -\frac{J^{Li}}{D} \tag{15}$$

where J^{Li} is the pore wall flux of lithium-ion in the electrolyte and D is the diffusion coefficient that influences the transfer of lithium-ion.

According to the radial diffusion equation and boundary condition, the lithium-ion concentration changes drastically at the surface of the electrode where the reactions take place and change slowly at the center of the spherical particle. Thus, the total electrode volume can be divided into two individual parts, one for the bulk (with subscript bulk) and one for the surface (with subscript surf) [30]. The concentration of lithium-ion is assumed as uniform distribution in the respective individual parts. With this assumption, the lithium-ion transformation can be described by Fick's first law. In the discharge process, lithium-ions transport from the surface of the negative electrode to the surface of the positive electrode. Meanwhile, lithium-ion in the electrode is transferred from bulk to surface in negative and surface to bulk in positive. So, (14) can be rewritten as one-dimensional formulation

$$J_{bs}^{Li} = D \frac{\left(c_{s,p,surf} - c_{s,p,bulk}\right)}{\delta_{bv}} \tag{16}$$

where J_{bs}^{Li} is the flux of lithium-ion for the interface between bulk and surface, δ_{bv} is the equivalent diffuse distance. According to (15), the charge number in the electrode surface and bulk can be expressed as

$$q_{s,p} = q_{s,p}^0 + (I - \dot{q})\, t \tag{17}$$

$$q_{b,p} = q_{b,p}^0 + \dot{q}t \tag{18}$$

where $q_{s,p}^0$ is the charge number in the electrode surface at initial time, $q_{s,p}^0$ is the charge number in the electrode bulk at initial time, $\dot{q}$ is the charge transfer velocity

$$\dot{q} = FAJ_{bs}^{Li} \tag{19}$$

For simplification, (19) can be rewritten as

$$\dot{q} = D_L \left(c_{s,p,surf} - c_{s,p,bulk}\right) \tag{20}$$

where $D_L = FAD/\delta_{bv}$ is a lumped diffusion coefficient. $c_{s,p,surf}$ and $c_{s,p,bulk}$ can be calculated by

$$c_{s,p,surf} = \frac{q_{s,p}}{Fv_{s,p}} \tag{21}$$

$$c_{s,p,bulk} = \frac{q_{b,p}}{Fv_{b,p}} \tag{22}$$

$$v_p = v_{s,p} + v_{b,p} \tag{23}$$

where $v_{b,p}$ is the volume of the positive electrode bulk part. Consequently, $c_{s,p,surf}$ can be calculated by (16)-(23) and finally obtain the θ_p from (2).

In the positive electrode, lithium-ion intercalate to electrode when battery discharge and de-intercalate to electrode when battery charge. The two different processes lead that D_L has different values under the process of intercalation and de-intercalation [33]. D_L is also a function of *SOH* and temperature [11]. In our research work, the effect of *SOH* is not considered, which may be studied in the future. Then, D_L can be described as (24) and the effect of battery inner temperature $f(T)$ will be discussed in Section III.C.

$$D_L = \begin{cases} D_c; & I < 0 \\ f(T) \cdot D_d; & I > 0 \end{cases} \tag{24}$$

where D_c is the diffusion coefficient in the charge process and D_d is the diffusion coefficient in the discharge process.

C. THERMAL DEPENDENT PARAMETERS

Arrhenius equation governs the most significant temperature-dependent parameters including diffusion coefficient and electrolyte ionic conductivity. So, the diffusion coefficient under the discharge process can be described as [14]

$$D_L = D_d \cdot e^{-\beta_D(1/T_{in} - 1/T_0)} \tag{25}$$

where β_D is the coefficient which is related to temperature, and T_{in} is the current inner temperature, T_0 is the standard temperature.

Resistance and *OCV* also follow Arrhenius equation. And because the effect of temperature to them is relatively minor, $R_\Omega(T)$ and $V_{\text{oc}}(T)$ can be simplified as linear equation [14]

$$R_\Omega(T) = R_{ref} + \alpha_r T_{in} \tag{26}$$

$$V_{oc}(T) = V_{ref} + \left(T_{in} - T_{ref}\right) \frac{\partial U_{oc}}{\partial T} \tag{27}$$

where R_{ref} and V_{ref} are the value of parameters at standard inner temperature, α_r is the temperature coefficient, and $\partial U_{\text{oc}}/\partial T$ is the entropic heat coefficient.

IV. THERMAL MODEL

A. HEAT GENERATION MODEL

For lithium-ion battery, temperature has significant impact on battery parameters such as resistance, diffusion coefficient, and reaction rate constants. During the charge or discharge process, the temperature may fluctuate in large range. So, the influence of temperature should be considered in battery model.

The main components that generation heat in lithium-ion battery include positive plate, separator and negative plate. And there are four heat sources: electrical losses, entropic heat, heat generated by side reaction, and heat of mixing [34]. Compared to other heat sources, heat generated by side reaction and heat of mixing are relatively minor, thus they are ignored in our proposed model. And the total heat sources considered here can be expressed by

$$\dot{Q}_{gen} = \dot{Q}_{irr} + \dot{Q}_{rev} \tag{28}$$

where $\dot{Q}_{irr}$ is the irreversible heat generated. It is quantified by how much the instantaneous cell potential deviates from the equilibrium potential, which is calculated by

$$\dot{Q}_{irr} = I\left(V_t - U_{oc}\right) = I^2 R_\Omega \tag{29}$$

the reversible heat generated $\dot{Q}_{rev}$ describes the change of entropic. It is usually calculated as the following

$$\dot{Q}_{rev} = I \cdot T_{in} \frac{\partial U_{oc}}{\partial T} \tag{30}$$

the entropic heat coefficient $\partial U_{\text{oc}}/\partial T$ is a function of *SOC* and it differs for different types of battery. A common way of calculating it is measuring the steady equilibrium potential at different temperature points and different *SOC* points [24]. Then, we can obtain $\partial U_{\text{oc}}/\partial T$ at any *SOC* by the look up table method.

B. TEMPERATURE MODEL

Distribution of temperature in battery is inhomogeneous. According to the second law of thermodynamics, the temperature is nearly uniform at the center of battery but changes drastically in the area near the surface. To accommodate this, we can assume that the total volume can be split into inner and surface and the temperature keeps uniformity in their own part. Consequently, the inner temperature can be described by the following equation

$$M \cdot C_b \frac{\partial T_{in}}{\partial t} = \dot{Q}_{gen} - h_s A_{surf}\left(T_{surf} - T_{amb}\right) \tag{31}$$

where M is the weight of battery, C_b is the specific heat, A_{surf} is the battery surface area, h_s is the convective heat transfer coefficient, T_{amb} is the ambient temperature and

T_{surf} is the surface temperature of battery. The relationship between inner temperature and surface temperature can be described as [35]

$$T_{in} = T_{surf}\,(1+\lambda) - T_{amb}\lambda \tag{32}$$

where λ is the ratio between heat transfer resistance inside the cell and heat transfer resistance outside the cell.

V. EXPERIMENTAL SETUP AND PARAMETERS IDENTIFICATION

A. BATTERY TEST BENCH

A battery test bench has been established to acquire measurement data such as load current, terminal voltage and ambient temperature. The configuration of the test bench is shown in Fig. 3, which consists of a battery test system BTS-2016CL (produced by WuHan LANDY electronic company) and a host computer for profile setting and data storage.

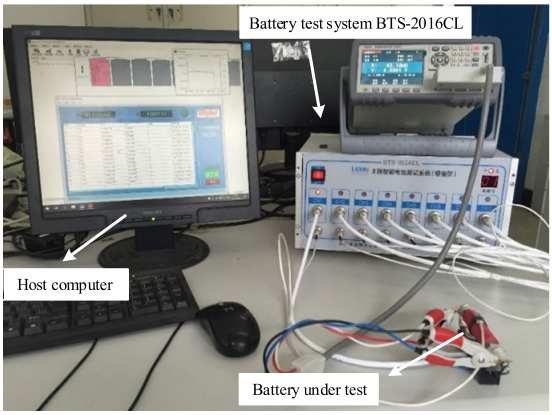

FIGURE 3. Battery test bench.

The battery used in this test is SANYO UR18650AA lithium-ion battery. Parameters of the battery are given in Table 1.

TABLE 1. Parameters of the battery under test (UR18650AA).

Parameters	Value
Nominal capacity	2.25 Ah
Nominal voltage	3.6 V
Charging cut-off voltage	4.2 V
Discharge cut-off voltage	2.75 V
Weight	43 g

B. EXPERIMENTAL PROCESS

In this paper, two main experimental setups are implemented. The first one is conducted on lithium-ion battery cell to parameterize, while the second one is used to validate the model of CTSPM. These experimental data could also be employed to estimate the parameters of Thevenin model and validate the advantages of our model.

In the first experimental setup, the necessary parameters for CTSPM will be obtained. As shown in Fig. 4, the operation of CTSPM needs four kinds of test to measure the necessary parameters like capacity, *OCV* curve, resistance curve, and dU/dT curve. Meanwhile it should provide data for estimating parameters like D_c, D_d, β_D, h_s, and C_b. To measure the *OCV-SOC* curve and the maximum discharge capacity, a complete discharge under 1/20C at ambient temperature is implemented. Then a hybrid pulse power characteristics (HPPC) test has been implemented to measure the *DCR-OCV* curve [36]. Besides a quiescent voltage test is conducted to obtain the $\partial U_{oc}/\partial T$-*SOC* curve [37]. In this study, the static voltage has been measured at six *SOC* points (100%, 70%, 55%, 35%, 20%, 0%) and three *AT* points (291K, 297K, 303K). These test results of SANYO battery are shown in Fig. 5(a-c). Diffusion coefficient is changed with *SOC* and it usually takes the average value. Then, the process of voltage recovery after discharge stop is equivalent to the charge process. So, an intermittent discharge process which includes four periods of constant current discharge processes and four periods of the standing process has been designed to estimate these parameters. Considering the CTSPM applied to low current and the effect of current and temperature, the intermittent discharge test has been implemented under different conditions (*AT*: 295K; *I*: 0.5C; *AT*: 295K, *I*: 1.0C; *AT*: 303K; *I*: 0.5C; *AT*: 303K; *I*: 1.0C). The corresponding response curves of voltage and temperature of intermittent discharge test are shown in Fig. 7(a-b) respectively.

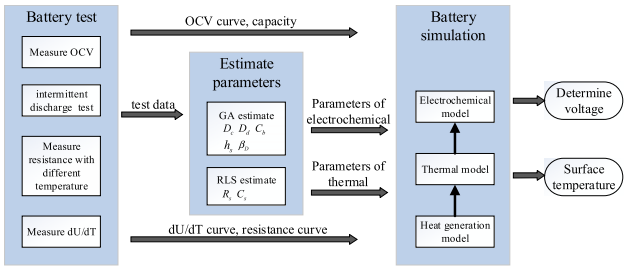

FIGURE 4. The application flow of CTSPM.

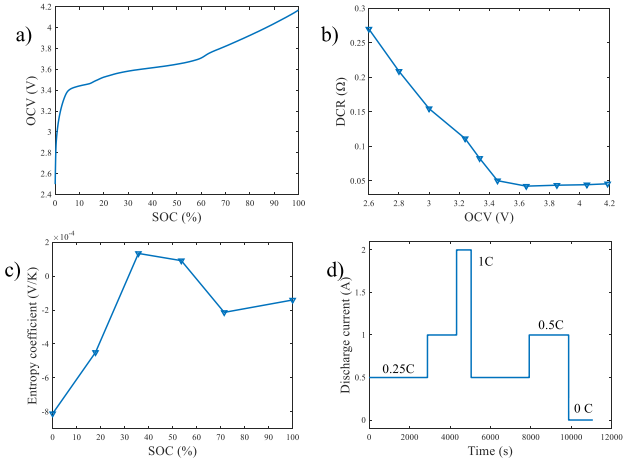

FIGURE 5. Current profile and parameters curve: (a) *OCV-SOC* curve; (b) *DCR-OCV* curve; (c) Entropy coefficient curves; (d) Current profile of DST test.

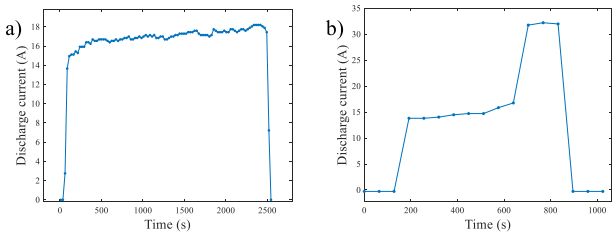

FIGURE 6. Satellite battery work profile: (a) GEO satellite discharge current. (b) LEO satellite discharge current.

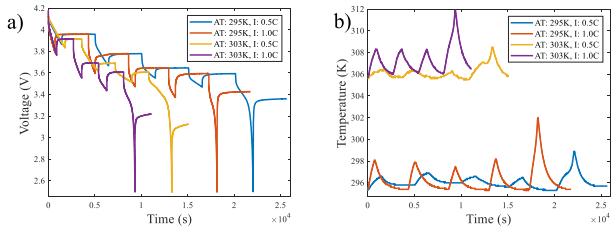

FIGURE 7. Data for GA estimation: (a) Voltage data; (b) Temperature data.

The second experimental setup is mainly used to validate the proposed model. As mentioned before, developing CTSPM is oriented by the application requirements of satellite batteries. Two main types of satellite, GEO satellite and LEO satellite has obviously different typical loads, as shown in Fig. 6 (a) and Fig. 6 (b), respectively. The load of GEO satellite is stable and the discharge current can be considered as constant. By contrast, the load of LEO satellite has changed obviously in the discharge process. Thus, the verification experiment is conducted by considering the following two cases: Case 1, constant stress test (CST); Case 2, dynamic stress test (DST).

CST is discharging a fully charged battery to cut-off of voltage. In this research, CST is executed under different constant current (0.5C and 1C) and ambient temperature (298K and 303K). It reflects the basic discharge performance and it is usually implemented for validating battery models. DST is used for observing the dynamic process of voltage change. It contains multi-segment of constant discharge current under constant ambient temperature (297K) and the load profile is shown in Fig. 5(d).

For comparison, the simulation results of one-order Thevenin model which is one of the common ECMs have been added. The ECM parameters polarization resistance R_s and polarization capacitance C_s are estimated by recursive least square (RLS). The values of each parameter and their sources are listed in Table 2. Ohmic resistance R_e is measured by interval discharge which lasts 10s with each terminal voltage descending 0.1V. The battery *OCV* and capacity are measured through constant-current discharge at 0.1A and they are also used for CTSPM.

C. THERMAL DEPENDENT PARAMETERS

Table 3 summarizes seven parameters of CTSPM model about electrochemistry. OCV curve and capacity can be measured through constant-current discharge with 0.05C at 297K,

TABLE 2. Thevenin-1RC model parameters.

Parameter	Symbol	Source	Value
Capacity	$C_{battery}$	Measure	2.215 Ah
OCV	U_{oc}	Measure	Fig. 5 (a)
Ohmic resistance	R_e	Measure	Fig. 5 (b)
Polarization resistance	R_s	Estimate	0.05163 Ω
Polarization capacitance	C_s	Estimate	2900.8 F

TABLE 3. Electrochemical parameters of CTSPM.

Parameter (in 297 K)	Symbol	Source	Value
Capacity	$C_{battery}$	Measure	2.215 Ah
OCV-SOC curve	U_{oc}	Measure	Fig. 5 (a)
DCR-SOC curve	R_e	Measure	Fig. 5 (b)
Diffusion coefficient for discharge	D_d	Estimate	0.5022 C·m^3 (mol· s)$^{-1}$
Diffusion coefficient for charge	D_c	Estimate	0.0502 C·m^3 (mol ·s)$^{-1}$
Electrode bulk volume	v_b	Ref [30]	3.15e-5 m^3
Electrode surface volume	v_s	Ref [30]	0.35e-5 m^3

while resistance can be measured through a specific discharge process at 297K as described in Section V.B. Lithium-ion diffusion coefficient is different for each cell and it cannot be measured for commercial battery. In fact, each discharge process corresponds to unique diffusion coefficient. So, the diffusion coefficient can be estimated by method of parameter optimization.

Table 4 lists six parameters about the temperature of CTSPM model. The temperature factor of capacity and resistance can be obtained through measuring the performance characteristics of battery under different ambient temperatures and calculating the parameters by the least square method. The temperature factors of diffusion are hard to measure directly for finished cells and can be estimated from experimental data as well. Otherwise, measuring the surface thermal conductivity, inner thermal conductivity and specific heat need special equipment which is beyond the ability of commonly used experiment bench, so these parameters are also needed to be estimated in this paper. It is an effective manner that using multi-parameter optimization methods like particle swarm optimization [38], harmony search [9] and genetic algorithm (GA) [39] to estimate battery parameters. By balancing the precision and computational cost, GA has been adopted to estimate these parameters with dynamic

TABLE 4. Temperature parameters of CTSPM.

Parameter	Symbol	Source	Value
Convective heat transfer coefficient	h_s	Estimate	23.19 W(m^{2}k)$^{-1}$
Ratio of heat transfer resistance inside and outside	λ	Ref [35]	0.33
Battery weight	M	Measure	0.043 kg
Specific heat	C_p	Estimate	1036.2 J(kg·K)$^{-1}$
Entropic heat coefficient	$\partial U_{oc}/\partial T$	Measure	Fig. 5 (c)
Temperature factor of resistance	α_r	Measure	0.025
Temperature factor of diffusion	β_D	Estimate	0.1475e-6

discharge current data. For GA, the variables include D_c, D_d, β_D, h_s, and C_b. The fitness function is

$$Obj\_Function = \min\left[(V_m - V_{GA})^2 + (T_m - T_{GA})^2\right] \quad (33)$$

where V_m is the measured battery voltage, T_m is the measured surface temperature, V_{GA} is the output voltage of CTSPM, and T_{GA} is the output surface temperature of CTSPM. To obtain V_{GA} and T_{GA}, the experiment data should be input to CTSPM which includes *OCV-SOC* curve, discharge current, and quantity. The other parameters of GA keep default in the optimization toolbox of MATLAB. In order to decrease the randomness of optimization results, the optimization process would be run five times and the averaged values are used [9].

VI. MODEL VALIDATION

A. UNDER CONSTANT CURRENT CONDITION

Constant current discharge is the basic working model of battery. Thus, we validate the performance of CTSPM under constant current discharge condition firstly, with the results described in Section V.B. Fig. 8 shows the comparison results between simulated data and experimental data under the operating condition of constant current discharge (0.5C, 1C) at typical ambient temperature (298K, 303K). Fig. 8(a) and Fig. 8(b) depict the voltage result under two discharge currents at 298K and 303K, respectively. The simulated voltage errors of CTSPM and Thevenin model to experimental data under 298K are shown in Fig. 8(c), while Fig. 8(d) shows the error results under 303K. It is indicated that the results estimated by CTSPM can match well with experimental results and are better than the results obtained by Thevenin model. Especially at low SOC, Thevenin model is unacceptable but CTSPM can still agree well with experimental results. Root Mean Square Error (RMSE) and Mean Absolute Error (MAE) are summarized in Table 5 and computational formulas of RMSE and MAE are given by (34)-(36). It is also clearly illustrated that CTSPM is much better than Thevenin under different operating conditions.

$$X_{error} = X_s - X_m \quad (34)$$

$$RMSE = \sqrt{\frac{1}{p}\sum_{i=1}^{p}\left(X^i_{error} - \bar{X}_{error}\right)^2} \quad (35)$$

$$MAE = \frac{1}{p}\sum_{i=1}^{p}\left|X^i_{error} - \bar{X}_{error}\right| \quad (36)$$

where X_s is the simulation value, X_m is the measurement value, while X_{error} refers to the error between simulation value and measurement value and $\bar{X}_{error}$ represents the mean of error.

The error of CTSPM increases evidently at low SOC. The possible reason is that the diffusion coefficient has changed and this parameter is assumed as constant in CTSPM. Otherwise, various diffusion coefficients and maximum store charge in battery lead to the increasing error at low SOC and this effect will be researched in future.

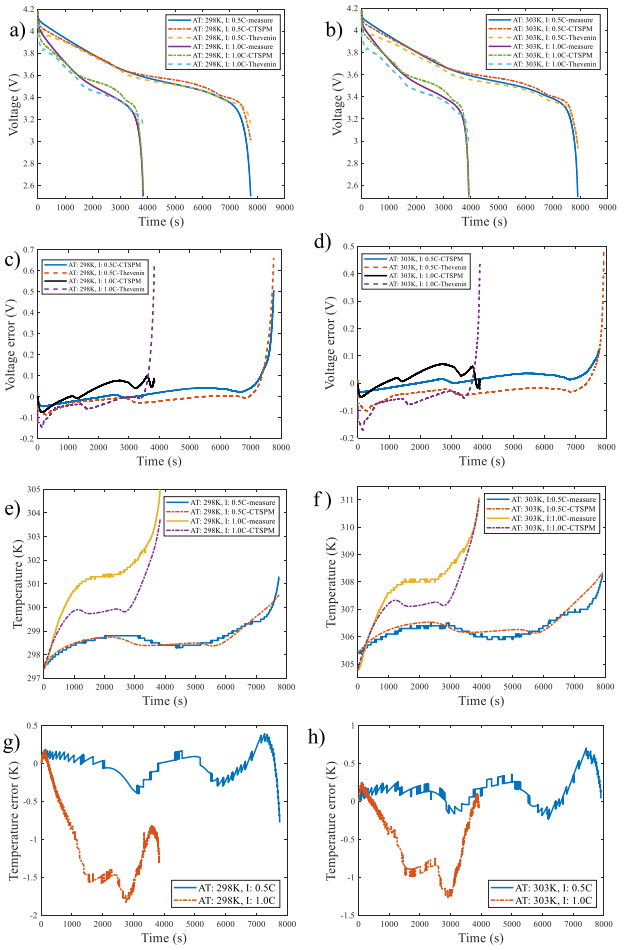

FIGURE 8. Simulation result for constant current conditions: (a) Terminal voltage at 298K; (b) Terminal voltage at 303K; (c) Terminal voltage at 298K; (d) Terminal voltage at 303K; (e) Surface temperature at 298K; (f) Surface temperature at 303K; (g) Surface temperature simulation error at 298K; (h) Surface temperature simulation error at 303K.

TABLE 5. The simulation error of voltage under constant operating conditions.

Operating conditions	RMSE (V)		MAE (V)	
	CTSPM	Thevenin	CTSPM	Thevenin
AT: 298K, *I*:0.5C	0.0619	0.0780	0.0354	0.0345
AT: 298K, *I*:1.0C	0.0523	0.0922	0.0451	0.0559
AT: 303K, *I*:0.5C	0.0438	0.0817	0.0263	0.0369
AT: 303K, *I*:1.0C	0.0416	0.0808	0.0356	0.0677

The simulation results of surface temperature under two current discharges are shown in Fig. 8(e) for 298K and in Fig. 8(f) for 303K. RMSE and MAE are summarized in Table 6. It clearly demonstrates that CTSPM can accurately simulate surface temperature variations of the experimental battery with maximum error of 0.3K under 0.5C discharge current. Under 1.0C discharge current, the error become larger especially for middle SOC but the error is still less than 1.5K.

B. UNDER DYNAMIC CURRENT CONDITION

The main advantage of CTSPM over ECM (one-order Thevenin model) is the ability of describing battery behavior

TABLE 6. The simulation error of temperature under constant operating conditions.

Operating conditions	RMSE (K)	MAE (K)
AT: 298K, *I*:0.5C	0.1703	0.1339
AT: 298K, *I*:1.0C	1.2286	1.1183
AT: 303K, *I*:0.5C	0.2327	0.1858
AT: 303K, *I*:1.0C	0.7101	0.5972

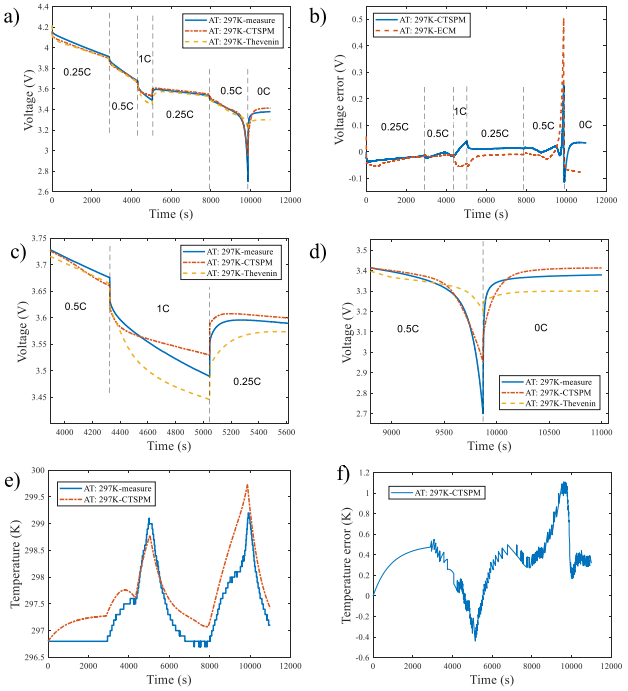

FIGURE 9. Simulation result for dynamic current conditions: (a) Terminal voltage at 297K; (b) Terminal voltage error at 297K; (c) Zoom out the third stage discharge curve; (d) Zoom out the sixth stage discharge curve; (e) Surface temperature at different temperature; (f) Surface temperature error.

under dynamic current condition. To verify this advantage, the experiments of dynamic discharge current have been designed and described in Section V.B, and the experiments are conducted under the ambient temperature of 297K. Corresponding experimental results and simulation results estimated by different methods are shown in Fig. 9. The voltage results are depicted in Fig. 9(a). and the voltage errors of CTSPM and Thevenin model under 297K are demonstrated in Fig. 9(b). The results indicate that the voltage estimated by proposed model matches well with experimental results, and they are superior to the results of Thevenin model. The voltage curves of third stage and sixth stage discharge process have been zoomed out in Fig. 9(c) and Fig. 9(d) respectively. After discharge current has changed, CTSPM has obvious advantage compared with Thevenin model. Especially, the estimation result of Thevenin model is not consistent with experimental data at low SOC as shown in Fig. 9(c). At the static process (0C), Thevenin model simulation also cannot reflect the process of self-recharge but the simulation results of CTSPM are still consistent with experimental results. The global RMSE and MAE are summarized in Table 7. The local RMSE and MAE which are defined as the discharge process within 10 minutes after current change are summarized in Table 8. Obviously, the error of CTSPM is reduced to about 1/3 that of Thevenin model. It obviously illustrates that CTSPM has better performance than Thevenin under dynamic current condition.

TABLE 7. The simulation error of voltage under dynamic operating conditions.

Operating conditions	RMSE (V)		MAE (V)	
	CTSPM	Thevenin	CTSPM	Thevenin
AT:297	0.0282	0.0493	0.0196	0.0318

TABLE 8. The simulation error of voltage after current change ten minutes.

Location of current change	RMSE (V)		MAE (V)	
	CTSPM	Thevenin	CTSPM	Thevenin
1st	0.0560	0.1975	0.0480	0.1750
2st	0.1065	0.4433	0.0911	0.3582
3st	0.1515	0.4219	0.1291	0.3689
4st	0.0466	0.2439	0.0381	0.2097
5st	0.0922	0.5004	0.0679	0.4481

The surface temperature simulation result under two ambient temperatures are shown in Fig. 9(e) and the error of temperature is shown in Fig. 9(f). RMSE and MAE are summarized in Table 9. It can be seen that, CTSPM can simulate surface temperature variations very close to experimental results with maximum error of 1K under 297K.

TABLE 9. The simulation error of temperature under dynamic operating conditions.

Operating conditions	RMSE (K)	MAE (K)
AT:297	0.4470	0.3884

Besides, CTSPM also has superior computational efficiency compared with ECM. In order to illustrate the computational cost of different models, CPU execution time is employed. The models are executed on a computer with Corel-i7 6800 processor, 8G RAM. The CTSPM and ECM are implemented using MATLAB 9.2. SP model and P2D model are based on COMSOL 5.2 which is more efficient than MATLAB in general, and the difference between these two softs is no significant effect on this research results. In this validation work, a discharge operating profile which includes 11,000 sampling points is designed and three kinds of battery model are simulated. The average simulation times of different models are presented in Table 10. It obvious that CTSPM has the highest computational efficiency.

TABLE 10. The simulation time of different models.

Model	CTSPM	Thevenin	SP	P2D
Time (s)	0.91	3.05	2	14

VII. CONCLUSION

In conclusion, CTSPM is presented for battery simulation under dynamic load condition, which maintains accurate estimation for terminal voltage and surface temperature over a broad range of ambient temperature and discharge rate. The electrochemical model neglects the electrolyte concentration difference and simplifies the electrode as a single particle similar with the SP model. Then, the lithium-ion diffusion transport is simplified as consistency diffusion between two regions. The temperature-dependent electrochemical model considers the variations in model parameters through Arrhenius equation. The proposed thermal model consists of two lumped thermal nodes interconnected by simplifying the thermal transfer model. The heat generation model considers two sources of heat during operation (irreversible losses and reversible losses). These two models (electrochemical and thermal model) are coupled together in an iterative fashion to predict cell terminal voltage and surface temperature accurately and efficiently. In addition, the application of the look-up table method decreases the error caused by data fitting.

The CTSPM is validated under the constant current at different current rates and temperatures. Then, this model is validated under the operating conditions of dynamic current. The parameters of CTSPM are obtained through direct measurement and estimation by GA. The validation results show that CTSPM has less error and higher efficiency than Thevenin model under different operating conditions. Compared with electrochemical model, CTSPM also has better parameter measurability and require less computation cost. Consequently, CTSPM may be a superior model that satisfies the real-time application requirements of satellite BMS.

ACKNOWLEDGMENT

The authors are very grateful to RiXing Wang for the inspiring discussions, and also would like to say thanks to the reviewers for their corrections and helpful recommendations.

REFERENCES

[1] X. Wang, Y. Sone, H. Naito, C. Yamada, G. Segami, and K. Kibe, "Cycle-life testing of 100-Ah class lithium-ion battery in a simulated geosynchronous-Earth-orbit satellite operation," *J. Power Sources*, vol. 160, no. 1, pp. 602–608, 2006, doi: 10.1016/j.jpowsour.2006.01.052.

[2] S. Dey, Y. Shi, K. Smith, A. Colclasure, and X. Li, "From battery cell to electrodes: Real-time estimation of charge and health of individual battery electrodes," *IEEE Trans. Ind. Electron.*, vol. 67, no. 3, pp. 2167–2175, Mar. 2019, doi: 10.1109/TIE.2019.2907514.

[3] Y. Gao, X. Zhang, Q. Cheng, B. Guo, and J. Yang, "Classification and review of the charging strategies for commercial lithium-ion batteries," *IEEE Access*, vol. 7, pp. 43511–43524, 2019, doi: 10.1109/ACCESS.2019.2906117.

[4] Z. Wei, J. Zhao, R. Xiong, G. Dong, J. Pou, and K. J. Tseng, "Online estimation of power capacity with noise effect attenuation for lithium-ion battery," *IEEE Trans. Ind. Electron.*, vol. 66, no. 7, pp. 5724–5735, Jul. 2019, doi: 10.1109/TIE.2018.2878122.

[5] R. Xiao, J. Shen, X. Li, W. Yan, E. Pan, and Z. Chen, "Comparisons of modeling and state of charge estimation for lithium-ion battery based on fractional order and integral order methods," *Energies*, vol. 9, no. 3, p. 184, 2016, doi: 10.3390/en9030184.

[6] A. Guha and A. Patra, "State of health estimation of lithium-ion batteries using capacity fade and internal resistance growth models," *IEEE Trans. Transport. Electrific.*, vol. 4, no. 1, pp. 135–146, Mar. 2018, doi: 10.1109/TTE.2017.2776558.

[7] Z. Yang, D. Patil, and B. Fahimi, "Electrothermal modeling of lithium-ion batteries for electric vehicles," *IEEE Trans. Veh. Technol.*, vol. 68, no. 1, pp. 170–179, Jan. 2019, doi: 10.1109/TVT.2018.2880138.

[8] V.-H. Duon, H. A. Bastawrous, and K. W. See, "Accurate approach to the temperature effect on state of charge estimation in the $LiFePO_4$ battery under dynamic load operation," *Appl. Energ.*, vol. 204, pp. 560–571, Oct. 2017, doi: 10.1016/j.apenergy.2017.07.056.

[9] H. Chun, M. Kim, J. Kim, K. Kim, J. Yu, T. Kim, and S. Han, "Adaptive exploration harmony search for effective parameter estimation in an electrochemical lithium-ion battery model," *IEEE Access*, vol. 7, pp. 131501–131511, 2019, doi: 10.1109/ACCESS.2019.2940968.

[10] M. Doyle, T. F. Fuller, and J. Newman, "Modeling of galvanostatic charge and discharge of the lithium/polymer/insertion cell," *J. Electrochem. Soc.*, vol. 140, no. 6, p. 1526, 1993, doi: 10.1149/1.2221597.

[11] V. Ramadesigan, P. W. C. Northrop, S. De, S. Santhanagopalan, R. D. Braatz, and V. R. Subramanian, "Modeling and simulation of lithium-ion batteries from a systems engineering perspective," *J. Electrochem. Soc.*, vol. 159, no. 3, pp. R31–R45, 2012, doi: 10.1149/2.018203jes.

[12] T.-S. Dao, C. P. Vyasarayani, and J. McPhee, "Simplification and order reduction of lithium-ion battery model based on porous-electrode theory," *J. Power Sources*, vol. 198, pp. 329–337, Jan. 2012, doi: 10.1016/j.jpowsour.2011.09.034.

[13] S. Yuan, L. Jiang, C. Yin, H. Wu, and X. Zhang, "A transfer function type of simplified electrochemical model with modified boundary conditions and Padé approximation for Li-ion battery: Part 1. Lithium concentration estimation," *J. Power Sources*, vol. 352, pp. 245–257, Jun. 2017, doi: 10.1016/j.jpowsour.2017.03.060.

[14] Y. Ma, X. Li, G. Li, Y. Hu, and Q. Bai, "SOC oriented electrochemical-thermal coupled modeling for lithium-ion battery," *IEEE Access*, vol. 7, pp. 156136–156149, 2019, doi: 10.1109/ACCESS.2019.2949357.

[15] S. J. Moura, F. B. Argomedo, R. Klein, A. Mirtabatabaei, and M. Krstic, "Battery state estimation for a single particle model with electrolyte dynamics," *IEEE Trans. Control Syst. Technol.*, vol. 25, no. 2, pp. 453–468, Mar. 2017, doi: 10.1109/TCST.2016.2571663.

[16] C. Zhu, X. Li, R. Lu, J. Xu, and G. Fan, "A comparative study of three electrochemical battery models with different operating conditions," in *Proc. IEEE Transp. Electrific. Conf. Expo, Asia–Pacific (ITEC Asia–Pacific)*, Aug. 2017, pp. 1–7.

[17] S. Santhanagopalan, Q. Guo, P. Ramadass, and R. E. White, "Review of models for predicting the cycling performance of lithium ion batteries," *J. Power Sources*, vol. 156, no. 2, pp. 620–628, 2006, doi: 10.1016/j.jpowsour.2005.05.070.

[18] J. Li, K. Adewuyi, N. Lotfi, R. G. Landers, and J. Park, "A single particle model with chemical/mechanical degradation physics for lithium ion battery state of health (SOH) estimation," *Appl. Energy*, vol. 212, pp. 1178–1190, Feb. 2018, doi: 10.1016/j.apenergy.2018.01.011.

[19] R. Ahmed, M. E. Sayed, I. Arasaratnam, J. Tjong, and S. Habibi, "Reduced-order electrochemical model parameters identification and SOC estimation for healthy and aged Li-ion batteries—Part I: Parameterization model development for healthy batteries," *IEEE J. Emerg. Sel. Topics Power Electron.*, vol. 2, no. 3, pp. 659–677, Sep. 2014, doi: 10.1109/JESTPE.2014.2331059.

[20] R. Ahmed, M. El Sayed, I. Arasaratnam, J. Tjong, and S. Habibi, "Reduced-order electrochemical model parameters identification and state of charge estimation for healthy and aged Li-ion batteries—Part II: Aged battery model and state of charge estimation," *IEEE J. Emerg. Sel. Topics Power Electron.*, vol. 2, no. 3, pp. 678–690, Sep. 2014, doi: 10.1109/JESTPE.2014.2331062.

[21] P. W. C. Northrop, V. Ramadesigan, S. De, and V. R. Subramanian, "Coordinate transformation, orthogonal collocation, model reformulation and simulation of electrochemical-thermal behavior of lithium-ion battery stacks," *J. Electrochem. Soc.*, vol. 158, no. 12, p. A1461, 2011, doi: 10.1149/2.058112jes.

[22] N. Damay, C. Forgez, M. Bichat, and G. Friedrich, "Thermal modeling of large prismatic $LiFePO_4$/graphite battery. Coupled thermal and heat generation models for characterization and simulation," *J. Power Sources*, vol. 283, pp. 37–45, Jun. 2015, doi: 10.1016/j.jpowsour.2015.02.091.

[23] Z. Wang, J. Ma, and L. Zhang, "Finite element thermal model and simulation for a cylindrical Li-ion battery," *IEEE Access*, vol. 5, pp. 15372–15379, 2017, doi: 10.1109/ACCESS.2017.2723436.
[24] M. Farag, H. Sweity, M. Fleckenstein, and S. Habibi, "Combined electrochemical, heat generation, and thermal model for large prismatic lithium-ion batteries in real-time applications," *J. Power Sources*, vol. 360, pp. 618–633, Aug. 2017, doi: 10.1016/j.jpowsour.2017.06.031.
[25] G. K. Prasad and C. D. Rahn, "Model based identification of aging parameters in lithium ion batteries," *J. Power Sources*, vol. 232, pp. 79–85, Jun. 2013, doi: 10.1016/j.jpowsour.2013.01.041.
[26] S. Liu, J. Jiang, W. Shi, Z. Ma, L. Y. Wang, and H. Guo, "Butler–volmer-equation-based electrical model for high-power lithium titanate batteries used in electric vehicles," *IEEE Trans. Ind. Electron.*, vol. 62, no. 12, pp. 7557–7568, Dec. 2015, doi: 10.1109/TIE.2015.2449776.
[27] X. Zhang, J. Lu, S. Yuan, J. Yang, and X. Zhou, "A novel method for identification of lithium-ion battery equivalent circuit model parameters considering electrochemical properties," *J. Power Sources*, vol. 345, pp. 21–29, Mar. 2017, doi: 10.1016/j.jpowsour.2017.01.126.
[28] V. R. Subramanian, V. Boovaragavan, and V. D. Diwakar, "Toward real-time simulation of physics based lithium-ion battery models," *Electrochem. Solid State Lett.*, vol. 10, no. 11, pp. A255–A260, 2007, doi: 10.1149/1.2776128.
[29] A. Romero-Becerril and L. Alvarez-Icaza, "Comparison of discretization methods applied to the single-particle model of lithium-ion batteries," *J. Power Sources*, vol. 196, no. 23, pp. 10267–10279, 2011, doi: 10.1016/j.jpowsour.2011.06.091.
[30] M. Daigle and C. Kulkarni, "Electrochemistry-based battery modeling for prognostics," in *Proc. PHM Soc.*, New Orleans, LA, USA, 2013.
[31] N. Lotfi, R. G. Landers, J. Li, and J. Park, "Reduced-order electrochemical model-based SOC observer with output model uncertainty estimation," *IEEE Trans. Control Syst. Technol.*, vol. 25, no. 4, pp. 1217–1230, Jun. 2017, doi: 10.1109/TCST.2016.2598764.
[32] D. Yang, Y. Wang, R. Pan, R. Chen, and Z. Chen, "State-of-health estimation for the lithium-ion battery based on support vector regression," *Appl. Energy*, vol. 227, pp. 273–283, Oct. 2018, doi: 10.1016/j.apenergy.2017.08.096.
[33] P. Kemper, S. E. Li, and D. Kum, "Simplification of pseudo two dimensional battery model using dynamic profile of lithium concentration," *J. Power Sources*, vol. 286, pp. 510–525, Jul. 2015, doi: 10.1016/j.jpowsour.2015.03.134.
[34] D. Bernardi, E. Pawlikowski, and J. Newman, "A general energy balance for battery systems," *J. Electrochem. Soc.*, vol. 132, no. 1, p. 5, 1985, doi: 10.1149/1.2113792.
[35] C. Forgez, D. V. Do, G. Friedrich, M. Morcrette, and C. Delacourt, "Thermal modeling of a cylindrical $LiFePO_4$/graphite lithium-ion battery," *J. Power Sources*, vol. 195, no. 9, pp. 2961–2968, 2010, doi: 10.1016/j.jpowsour.2009.10.105.
[36] G. Giordano, V. Klass, M. Behm, G. Lindbergh, and J. Sjöberg, "Model-based lithium-ion battery resistance estimation from electric vehicle operating data," *IEEE Trans. Veh. Technol.*, vol. 67, no. 5, pp. 3720–3728, May 2018, doi: 10.1109/TVT.2018.2796723.
[37] A. Eddahech, O. Briat, and J.-M. Vinassa, "Lithium-ion battery heat generation investigation based on calorimetric entropy measurements," in *Proc. IEEE-ISIE*, Taipei, Taiwan, May 2013, pp. 1–5.
[38] H. M. Usman, S. Mukhopadhyay, and H. Rehman, "Universal adaptive stabilizer based optimization for Li-ion battery model parameters estimation: An experimental study," *IEEE Access*, vol. 6, pp. 49546–49562, 2018, doi: 10.1109/ACCESS.2018.2867560.
[39] J. Lu, Z. Chen, Y. Yang, and M. Lv, "Online estimation of state of power for lithium-ion batteries in electric vehicles using genetic algorithm," *IEEE Access*, vol. 6, pp. 20868–20880, 2018, doi: 10.1109/ACCESS.2018.2824559.

JINGLONG CHEN received the B.S. and M.S. degrees in mechanics from the Harbin Institute of Technology, Harbin, China, in 2012 and 2014, respectively, where he is currently pursuing the Ph.D. degree with the Deep Space Exploration Research Center.

His research interests include battery state estimation, satellite fault diagnosis method, and satellite prognostics and health management.

RIXIN WANG received the B.E. and M.E. degrees in computer science and the Ph.D. degree in spacecraft design the Harbin University of Science and Technology, Harbin, China, in 1985, 1991, and 2003, respectively.

He is currently an Associate Professor with the Department of Engineering Mechanics, Harbin Institute of Technology. His research interests include fault detection and diagnosis for machinery and spacecraft.

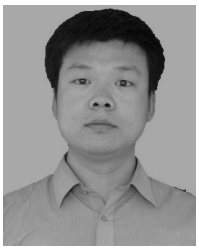

YUQING LI received the B.E. degree in mechanical design manufacturing and automation and the M.E. and Ph.D. degrees in general mechanics from the Harbin Institute of Technology, Harbin, China, in 2002, 2004, and 2008, respectively.

He is currently an Associate Professor with the Harbin Institute of Technology. His main research interests are planning and scheduling of spacecraft and spacecraft fault detection and diagnosis.

MINQIANG XU received the B.E. degree in electronics from Peking University, Beijing, China, in 1983, the M.E. degree in nuclear physics from Northeast Normal University, Changchun, China, in 1989, and the Ph.D. degree in general and fundamental mechanics from the Harbin Institute of Technology, Harbin, China, in 1999.

Since 2000, he has been a Professor with the Harbin Institute of Technology. His research interests include machinery and spacecraft fault detection and diagnosis, signal processing, and space debris modeling.